Quadrilateral and Hexahedral Mesh Generation Based on Surface Foliation Theory

Na Lei[a,d], Xiaopeng Zheng[c], Jian Jiang[b], Yu-Yao Lin[b], David Xianfeng Gu[b,d,*]

[a]*School of Software and Technology, Dalian University of Technology, Dalian China*
[b]*Comupter Science Department, Stony Brook University, New York*
[c]*School of Mathematics, Jilin University, Changchun China*
[d]*Beijing Advanced Innovation Center for Imaging Technology, Captial Normal University, Beijing China*

Abstract

For the purpose of isogeometric analysis, one of the most common ways is to construct structured hexahedral meshes, which have regular tensor product structure, and fit them by volumetric T-Splines. This theoretic work proposes a novel surface quadrilateral meshing method, *colorable quad-mesh*, which leads to the structured hexahedral mesh of the enclosed volume for high genus surfaces.

The work proves the equivalence relations among colorable quad-meshes, finite measured foliations and Strebel differentials on surfaces. This trinity theorem lays down the theoretic foundation for quadrilateral/hexahedral mesh generation, and leads to practical, automatic algorithms.

The work proposes the following algorithm: the user inputs a set of disjoint, simple loops on a high genus surface, and specifies a height parameter for each loop; a unique Strebel differential is computed with the combinatorial type and the heights prescribed by the user's input; the Strebel differential assigns a flat metric on the surface and decomposes the surface into cylinders; a colorable quad-mesh is generated by splitting each cylinder into two quadrilaterals, followed by subdivision; the surface cylindrical decomposition is extended inward to produce a solid cylindrical decomposition of the volume; the hexadhedral meshing is generated for each volumetric cylinder and then glued together to

*Corresponding author
Email address: gu@cs.stonybrook.edu (David Xianfeng Gu)

form a globally consistent hex-mesh.

The method is rigorous, geometric, automatic and conformal to the geometry. This work focuses on the theoretic aspects of the framework, the algorithmic details and practical evaluations will be given in the future expositions.

Keywords: Hexahedral mesh, Quadrilateral mesh, Foliation, Strebel Differential

1. Introduction

1.1. Motivation

Mesh generation plays a fundamental role in Computer Aided Design (CAD) and Computer Aided Engineering (CAE) fields . Finite Element Method (FEM) requires the input solids to be tessellated with high qualities. *There are mainly three types of volumetric meshing, the unstructured tetrahedral meshing, the unstructured hexahedral meshing and the structured hexahedral meshing.* Comparing to tetrahedral meshes, hexahedron mesh has many advantages [1]. The most important benefits are higher numerical accuracy, lower spacial complexity and higher efficiency:

- Non-uniform scaling hexahedra has much greater numerical accuracy compared to tetrahedra [2].
- The number of elements of a hexahedral mesh is four to ten times less than that of a tetrahedral mesh with the complexity of the input mesh being constant [2].
- Numerical computations on hexahedral meshes are up to 75% less memory and time consuming in comparison to tetrahedral meshes [3].

Automatic tetrahedral mesh generation is relatively mature, there exists reliable tools to generate high quality tetrahedral mesh automatically [4]. In contrast, automatic hexahedral mesh generation remains a great challenge, which is the so-called "holy grid" problem [2].

Recent years have witnessed the rapid development of the methodology of isogeometric analysis [5], [6]. In Computer Aided Design (CAD) field, the geometric shapes are represented as Spline surfaces/solids. The most prominent Spline schemes are T-Splines [7]. In Computer Aided Engineering (CAE) field, the isoparametric philosophy represents the solution space for dependent variables in terms of the same functions which represent the geometry. In reverse engineering field [8], shapes in real life are often acquired by 3D scanning technologies and represented as point clouds. The point cloud is triangulated to generate the boundary surface, the tetrahedral mesh is generated to tessellate the interior using automatic tetrahedral meshing generation tools. In order to apply isogeometric analysis method, the solid needs to be parameterized and fitted by volumetric Splines.The hexahedral meshes for isogeometric analysis are required to have **tensor product structure** locally, and with minimal number of singular vertices or line segments.

There are different approaches for hexahedral mesh generation. One approach is to construct a quadrilateral mesh for the boundary surface, then extend the boundary mesh into the interior, and construct a hexahedral mesh for the entire solid. The main problem the current work focuses on is as follows:

Given a closed surface S, with minimal user input, automatically construct a quadrilateral mesh $\mathcal{Q}$ on S, and extend $\mathcal{Q}$ to a hexahedral mesh of the enclosed volume. Both the quadrilateral and hexahedral meshes are with local tensor product structures, and the least number of singular vertices and singulary lines.

1.2. Non-structured Hex-Meshing

First, we consider general non-structured hex-meshing, which doesn't require the hex-mesh to have local tensor-product structure. The topological conditions for extending a quad-mesh to such a hex-mesh has been fully studied.

Definition 1.1 (Extendable Quad-Mesh)**.** *Suppose Ω is a volumetric domain in $\mathbb{R}^3$, $\mathcal{Q}$ is a topological quad-mesh of its boundary surface $\partial\Omega$. If $\mathcal{Q}$ is the boundary of a topological hex-mesh of Ω, then we say $\mathcal{Q}$ is* extendable.

One intriguing problem is to find the sufficient and necessary condition for a quadrilateral surface mesh to be extendable. Thurston [9] and Mitchel [10] proved that for a genus zero closed surface, a quadrilateral mesh is extendable if and only if it has even number of cells, furthermore Mitchel generalized the result to high genus surface cases [10]. Eppstein [11] used this existence result and proved that a linear number of hexahedra (in the number of quadrilaterals) are sufficient in such cases.

Recently, the results of Thurston, Mitchel and Eppstein have been generalized by Erickson in [12]. Erickson considers the homology of the volume (with $\mathbb{Z}_2$ coefficients), and proved the odd-cycle criterion for extendable quad-meshes:

Theorem 1.2 (Erickson 2014[12])**.** *Let Ω be a compact subset of $\mathbb{R}^3$ whose boundary $\partial\Omega$ is a (possibly disconnected) 2-manifold, and let $\mathcal{Q}$ be a topological quad mesh of $\partial\Omega$ with an even number of facets. The following conditions are equivalent:*

1. *$\mathcal{Q}$ is the boundary of a topological hex mesh of Ω.*
2. *Every subgraph of $\mathcal{Q}$ that is null-homologous in Ω has an even number of edges.*
3. *The dual curve arrangement $\tilde{\mathcal{Q}}$ is null-homologous in Ω.*

The concept of spacial twist continuum (STC) plays an important role in hexahedral mesh generation from a quadrilateral mesh. Given a quadrilateral mesh $\mathcal{Q}$, we construct its combinatorial dual $\tilde{\mathcal{Q}}$, and connect each pair of edges in $\tilde{\mathcal{Q}}$, which are dual to the opposite edges in a quad-face in $\mathcal{Q}$. Each connected component is called a *STC chord*. On a closed surface, all STC chords are loops. Müller-Hannemann [13, 14], Folwell and Mitchel [15] proposed to use curve contraction method for hexahedral mesh generation from quadrilateral meshes without self-intersecting STC loops. Erickson [12] gave a constructive proof which leads to an algorithm to produce a hex-mesh from an extendable quad-mesh.

1.3. Structured Hex-Meshing

For the purpose of isogeometric analysis, the surface and volume are generally represented as T-Splines. The surface T-Spline should be the restriction of the volume T-Spline on the boundary. This requires the **more structured** surface quad-mesh and volume hex-mesh, namely, the meshes have tensor product structure as global as possible. In this work, we focus on studying structured hex-meshing.

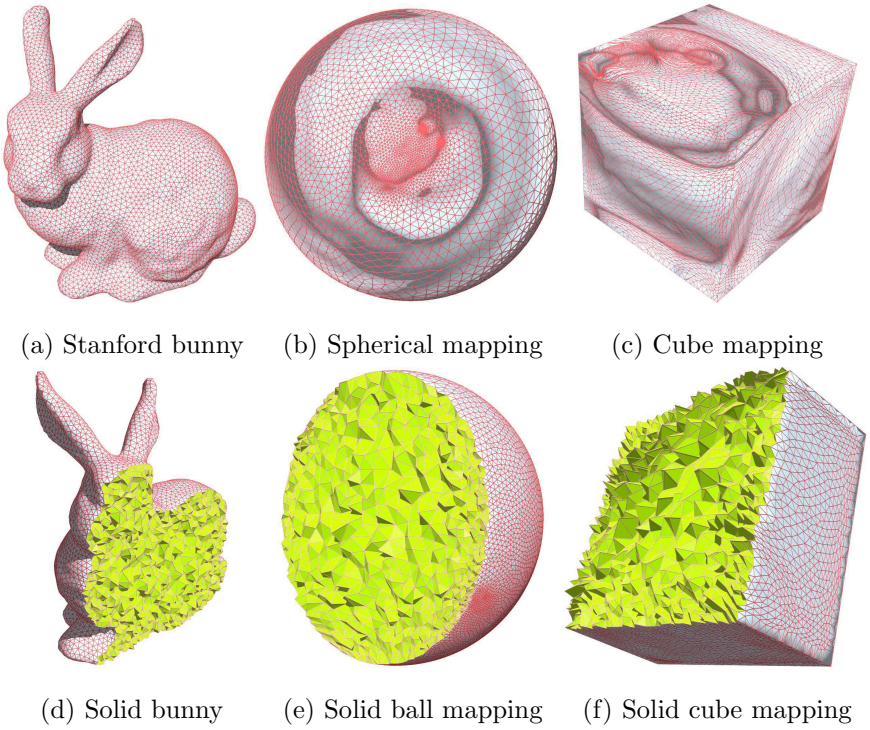

(a) Stanford bunny (b) Spherical mapping (c) Cube mapping

(d) Solid bunny (e) Solid ball mapping (f) Solid cube mapping

Figure 1: A solid with a genus zero boundary surface can be mapped onto a solid cube, using the method in [16].

1.3.1. Genus Zero Case

As shown in Fig. 1, given a solid ball Ω embedded in $\mathbb{R}^3$, its boundary surface $S = \partial\Omega$ is a closed surface with the induced Euclidean metric. According to surface uniformization theorem [17], if the genus of S is zero (a), then S can be conformally mapped onto the unit sphere (b), then to the unit cube (c).

The cube is an extendable quad-mesh, therefore the hexahedral mesh can be constructed for the interior solid. In fact, the boundary map can be extended into the interior, the solid can be mapped onto the solid ball diffeomorphically (e) and the solid cube (f). The hexahedral mesh can be constructed on the solid cube directly, then pull back to the input solid.

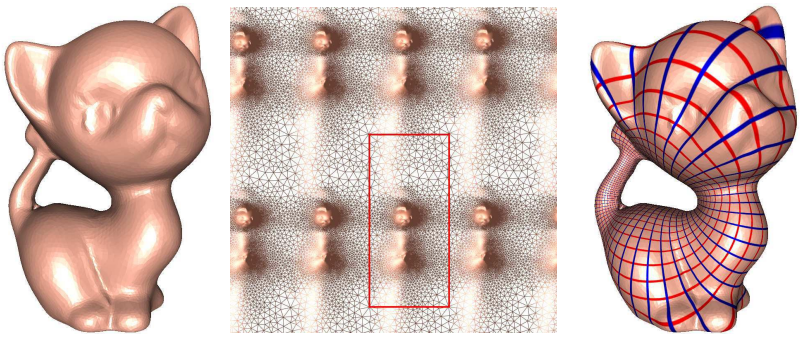

(a) Kitten surface (b) Flat torus (c) Quadrilateral mesh

Figure 2: A genus one closed surface can be conformally and periodically mapped onto the plane, each fundamental domain is a parallelogram. The subidvision of the parallelogram induces a extendable quad-mesh of the surface.

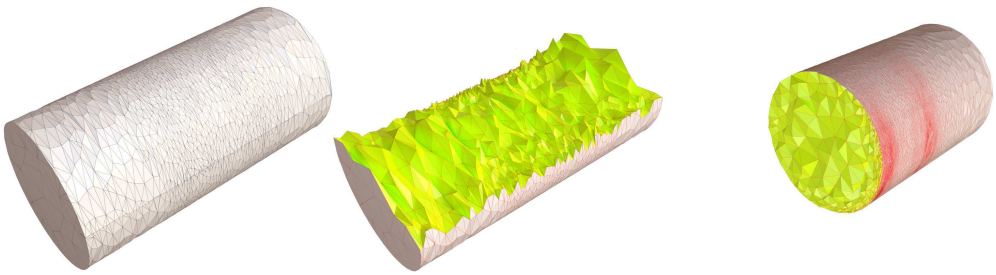

Figure 3: The interior of the kitten surface in Fig. 2 is mapped onto a canonical solid cylinder.

1.3.2. Genus One Case

As shown in Fig. 2, a genus one closed surface (a) can be conformally mapped onto a flat torus $\mathbb{E}^2/\Gamma$, where Γ is a lattice

$$\Gamma := \{m + n\eta | m, n \in \mathbb{Z}, \eta \in \mathbb{C}\},$$

according to surface uniformization theorem [17]. Each fundamental domain is a parallelogram (b). We subdivide the parallelogram to obtain a regular quadrilateral mesh $\mathcal{Q}$ (c), where $\mathcal{Q}$ is extendable. Then the interior volume of the Kitten surface is mapped onto a canonical solid cylinder in Fig. 3.

Therefore, in the following discussion, we only focus on surfaces with genus greater than one.

1.3.3. High Genus Cases: Trinity

For high genus surfaces, we introduce the concept of *red-blue quad mesh* or *colorable quad-mesh*.

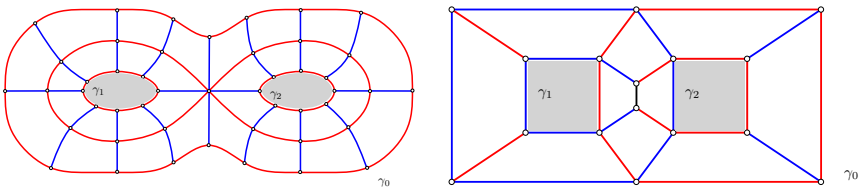

(a) Colorable quad-mesh. (b) Non-colorable quad-mesh

Figure 4: Quadrilateral meshes of a multiply connected planar domain. The left quad mesh is colorable, the right one is non-colorable.

Definition 1.3 (Colorable Quad-Mesh)**.** *A quad-mesh $\mathcal{Q}$ on a compact surface with genus greater than* 0 *is called* colorable*, if the edges of $\mathcal{Q}$ are colored in either red or blue, such that each quad-face has two opposite red edges and two opposite blue edges.*

As shown in Fig. 4, the left frame is a colorable quad-mesh of a multiply connected planar domain; the right frame shows a non-colorable quad-mesh.

A *foliation* $\mathcal{F}$ of S is a local product structure as shown in Fig. 5. That is, at each regular point $p \in S$, there exists a neighborhood U and a diffeomorphism $U \to \mathbb{R} \times \mathbb{R}$ such that the overlap maps take each $p \times \mathbb{R}$ to some $q \times \mathbb{R}$. The equivalence classes generated by the relation of lying in the same $p \times \mathbb{R}$ are the leaves of the foliation. One can associate a measure μ with a foliation $\mathcal{F}$, for an arc γ transverse to leaves, $\mu(\gamma)$ represents how many leaves the arc γ crosses.

Figure 5: A finite measured foliation on a genus three surface.

The pair $(\mathcal{F}, \mu)$ is called a *measured foliation*. If all the leaves are finite loops, the foliation is called a *finite measured foliation*.

All surfaces in real life are Riemann surfaces, which has complex local coordinate chart. On a Riemann surface S, a *holomorphic quadratic differential* Φ has local representation $\Phi = \varphi(z)dz^2$, where $\varphi(z)$ is a holomorphic function. A holomorphic quadratic differential induces a local complex coordinates $\zeta(p) = \int^p \sqrt{\varphi(\zeta)}d\zeta$ in neighborhoods away zeros, the horizontal parametric lines $\{\mathrm{Re}(\zeta) = \mathrm{const}\}$ define a foliation of S, the vertical coordinate gives the measure to the foliation. Therefore, a holomorphic quadratic differential induces a measured horizontal foliation $\mathcal{F}_\Phi$. If the measured foliation $\mathcal{F}_\Phi$ is finite, then Φ is called a *Strebel differential*.

The goal of the current work is to prove the following three concepts are equivalent

$$\{\text{Colorable Quad-Mesh}\} \leftrightarrow \{\text{Finite Measured Foliation}\} \leftrightarrow \{\text{Strebel Differential}\}.$$

which is called the *trinity relation*, as summarized in the main theorem:

Theorem 1.4 (Trinity)**.** *Suppose S is a closed Riemann surface with genus greater than one. Given an colorable quadrilateral mesh $\mathcal{Q}$, there is a finite measured foliation $(\mathcal{F}_\mathcal{Q}, \mu_\mathcal{Q})$ induced by $\mathcal{Q}$, and there exits a unique Strebel dif-*

ferent Φ*, such that the horizontal measured foliation induced by* Φ*,* $(\mathcal{F}_\Phi, \mu_\Phi)$ *is equivalent to* $(\mathcal{F}_\mathcal{Q}, \mu_\mathcal{Q})$*.*

Inversely, given a Strebel differential Φ*, it is associated with a finite measured foliation* $(\mathcal{F}_\Phi, \mu_\Phi)$*, and induces a colorable quadrilateral mesh* $\mathcal{Q}$*.*

This theoretic framework allows us to use the Strebel differentials to construct colorable quad-meshes, then extend to hexahedral meshes of the interior. The Strebel differentials can be constructed by variational method directly. This gives us a practical way to generate all possible colorable quad-meshes on a surface, and an automatic method for hexahedral mesh generation.

1.4. Pipeline

Figures 6 and 7 illustrate our proposed pipeline. *The input to the algorithm is the boundary surface of the volume, which is represented by either a CAD model or a triangle mesh. We assume the surface is converted to a triangle mesh, which is a closed manifold with genus* $g > 1$ *as shown in (a). The user input includes* $3g - 3$ *disjoint loops, namely an admissible curve system as defined in Def 5.2, and* $3g - 3$ *positive real numbers.* A Strebel differential is constructed automatically based on the user input as shown in (c), which leads to a colorable (red-blue) quad-mesh (e). The critical trajectories of the Strebal differential segment the surface into $3g - 3$ cylinders with quad-meshes (b), (d) and (f). The volume inside each cylinder surface is mapped onto a canonical solid cylinder with a hexahedral mesh, the mapping pulls back the hexahedral mesh to the original volume to produce the hexahedral mesh of the input solid, as shown in 7. The hexahedral mesh has local tensor product structure, with $2g - 2$ singular lines.

1.5. Contributions

This work bridges the quadrilateral and hexahedral meshing with measured foliations and holomorphic differentials, the theoretic framework leads to a con-

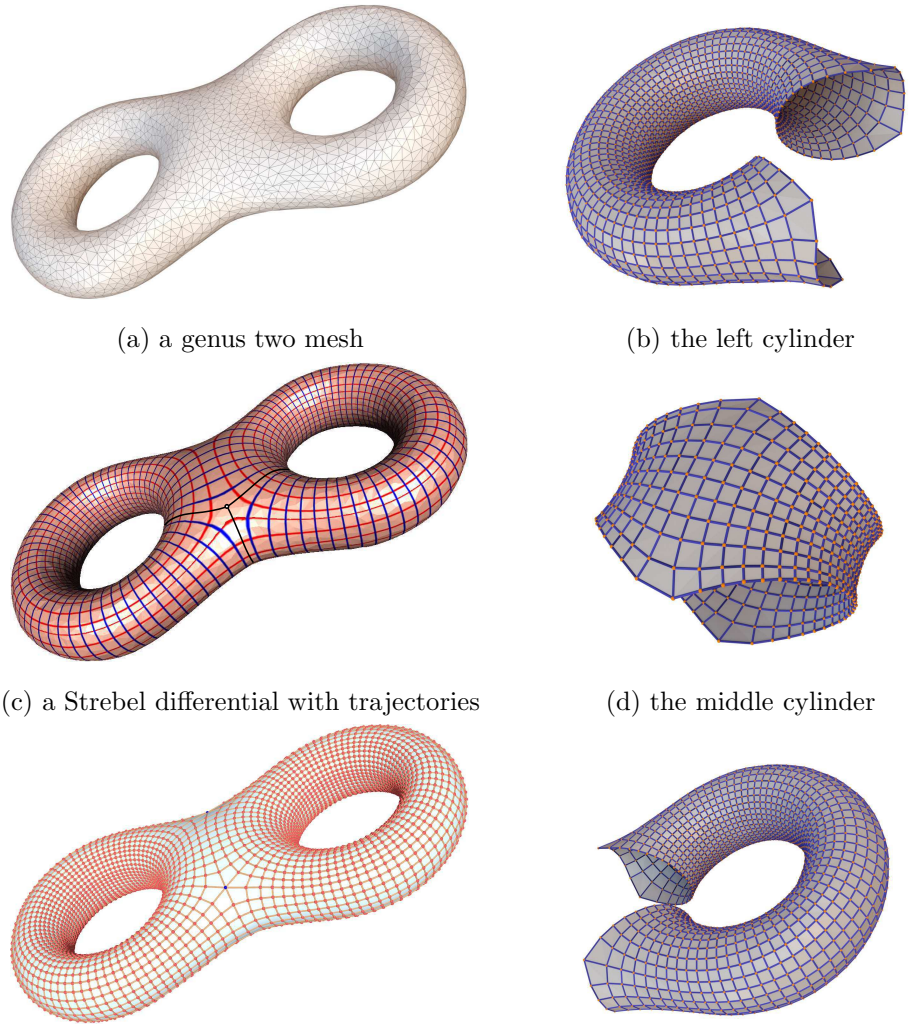

(a) a genus two mesh (b) the left cylinder

(c) a Strebel differential with trajectories (d) the middle cylinder

(e) the quad mesh induced by (c) (f) the right cylinder

Figure 6: A Strebel differential (c) on a genus two surface (a) induces a quad meshing (e); the horizontal, vertical trajectories are shown as red and blue curves in (c); the critical horizontal trajectories are labeled as black curves in (c). The surface is segmented into three cylinders (b),(d), (f) by slicing along the critical horizontal trajectories.

165 structive algorithm for quadrilateral and hexahedral mesh generations. It has the following merits:

1. *Rigorous* This framework lays down a solid theoretic foundation for struc-

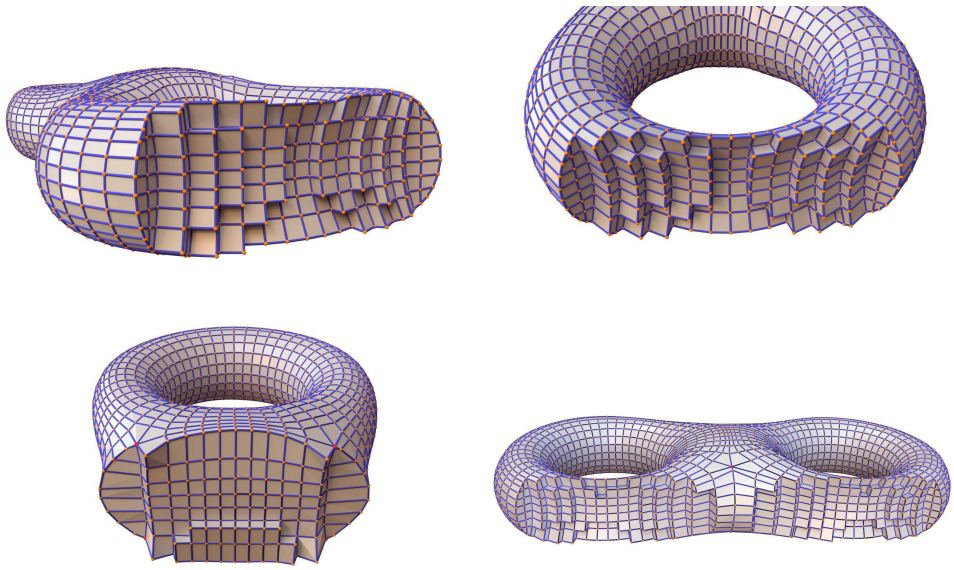

Figure 7: The hexahedral mesh of the solid induced by the quadrilateral mesh on the surface.

tured quadrilateral and hexahedral mesh generation.

2. *Automatic* The algorithm pipeline requires minimal user input, only $3g-3$ loops and $3g-3$ positive numbers. All the other steps of computations are automatic.

3. *Geometric* The quadrilateral and hexahedral meshing methods are geometric, not only topological/combinatorial.

4. *Regular* The hexahedral meshes have very regular tensor product structures with $2g-2$ singular lines, which is valuable for constructing volumetric/surface T-Splines.

5. *Conformal* The quadrilateral meshes are produces by the horizontal foliations of a Strebel differential, therefore, the shapes of quad-faces are with minimal angle distortions. This improves the robustness and numerical stability/accuracy for downstream analysis.

The work is organized as follows: Section 2 briefly review the related works; Section 3 explains the prerequisites and basic terminologies. Readers familiar

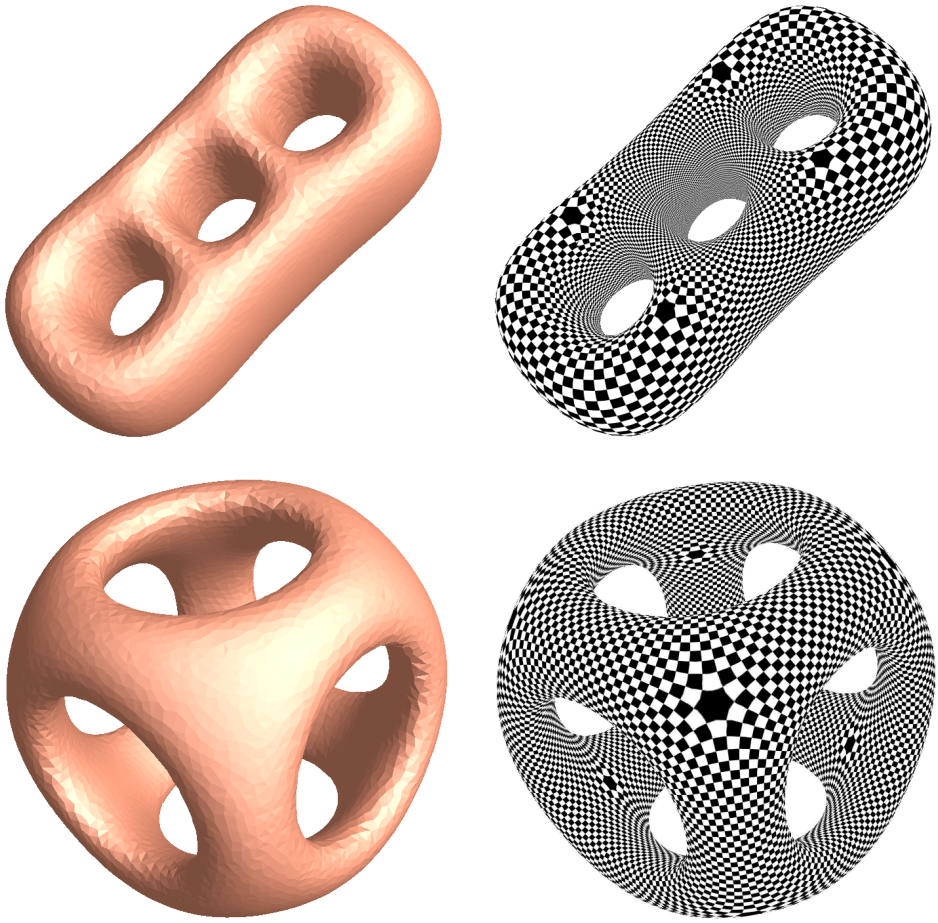

Figure 8: Two conjugate Strebel differentials induce quad-meshes on a genus 3 mesh (top row) and a genus 5 mesh (bottom row).

with Riemann surface theory can skip this section; Section 4 proves a colorable quad-mesh induces a foliation, and then a Strebel differential; Section 5 proves a
185 Strebel differential produces a colorable quad-mesh; the main theorem is summarized in Section 6; Section 7 discusses the topological aspects of the framework and the future directions; the work concludes in Section 8.

This work involves complex symbols and advanced mathematical concepts, we summarize all the main symbols in the table 1.

S	a compact Riemann surface embedded in $\mathbb{R}^3$
$\mathcal{I}$	the volume inside S
$\mathcal{O}$	the volume outside S
$(\mathcal{F}, \mu)$	a measured foliation
Φ	a holomorphic quadratic differential, generally a Strebel differential
ζ	natural coordinates of Φ
$\|\Phi\|$	the flat metric with cone singularities induced by Φ
z_i	zeros of a holomorphic quadratic differential Φ
$\mathcal{Q}_\Phi$	a quadrilateral mesh on S induced by a Strebel differential
C_k	a cylinder obtained by cutting S by the critical graph of Φ
h_k	the height of cylinder C_k
τ_i	edges on $\mathcal{Q}_\Phi$ on critical graph of Φ
σ_j	edges on $\mathcal{Q}_\Phi$ connecting zeros inside each cylinder
γ	simple loop
Γ	an admissible curve system
G_Γ	pants decomposition graph induced by an admissible curve system
θ	Dehn twisting angle
(G, h, l, θ)	poly-cylinder surface model
D_i	cutting half-disk
d	singular line, connecting two zeros

Table 1: Symbol List

2. Previous Works

The literature for quadrilateral and hexahedral meshing is vast, a complete review is beyond the scope of the current work, we refer readers to [2] for a thorough overview. In the following, we only briefly review some of the most related existing hex-meshing approaches.

The "sweeping" approach [18, 19] builds hexahedral mesh primitives by sweeping a surface quad-mesh along an arbitrary path generating hexahedral meshes with constant cross-section topology. This method requires the volume can be decomposed into a direct product of the surface and the path. The decomposition usually requires high manual efforts for complex shapes.

The "decomposition" or "multi-sweeping" approach generates hexahedral meshes by decomposing the original surface mesh into several simpler units. The decomposition can be performed using geometric decompositions as in [20, 21], or integrally during the meshing process by using an interior mesh as the cutting mechanism [22, 23, 24, 25]. This approach needs manual multilevel shape detection for the decomposition.

The "advancing front" approach generates a hexahedral mesh from the boundary of the surface mesh inward, such as the plastering method [26], harmonic field method [27]. These methods propagate the singularities to the medial axes of the volume which might lead to non-hexahedral shaped elements. The whisker weaving method [15] [28] converts the surface mesh to its dual STC and then generates a connectivity of the hexahedral elements in the enclosed 3D volume. Geometric information is incorporated for the whisker weaving method in [29].

The "frame field" approach builds smooth frame field, the hexahedral mesh is extracted from the field [30, 31, 32]. The method in [32] constructs three transversal vector fields in the volume, then these vector field is lifted to a branch covering space to merge into one vector field, the field is smoothed out by Hodge decomposition then project back to a sufficiently smooth frame field. These methods have limitations: the automatic generation of frame fields with

prescribed singularity structure is unsolved. The low quality frame fields may lead to invalid hexahedral meshes. *The theoretic analysis for the singular structure hasn't been established. Our proposed method is based on foliations, which is a generalization of vector field. Namely, a vector field induces a foliation, but a general foliation can not be represented by a vector field. Furthermore, the singular structure in the hex-mesh produced by our method has been analyzed completely. The heuristic method proposed in vector-field based method cannot handle complicated geometries, our method is more robust to deal with handle-bodies with theoretic guarantee.*

In "grid-based" approaches, the embedding space of the given model is first decomposed into a set of cells, which will then be projected or deformed to conform to the boundary geometry of the model. Marechal [33] proposed to generate hex meshes through an octree-based method through dual mesh generation and buffer-layers insertion. Ito et al. [34] developed a set of templates to optimize the octree-based hex meshing. Levy and Liu [35] introduced L^p centroidal tessellation to generate anisotropic hex-dominant meshes. One of the drawbacks of octree-based approaches is its pose-sensitivity, a small orientation change of the input model can produce different meshing results.

The "polycube-based" methods map the input model to a regular domain, then transfer the hexahedral grid (induced from the regular domain) back to the model. Due to its natural regularity and geometric similarity to the model, the polycube can be a suitable canonical domain for hex mesh generation [36, 37]. Singularity curves inside the polycube domain can be introduced to reduce the distortion [38, 39, 40]. Challenges of these volumetric parameterizations in hexahedral meshing are that either the cross-frame fields need to be given manually [38] or they need to be solved through expensive optimizations [39, 40], that cannot guarantee the finding of valid solutions.

All these methods require manual input and the resulting hexahedral meshes might not have local tensor product structure, the user lacks direct control of singularity structures. In our proposed approach, the user input is minimal, and the whole process can be automatic, the hexahedral meshes are structured

as tensor product everywhere, except at the $2g-2$ singular lines.

3. Prerequisites and Terminologies

Our proposed method is based on fundamental concepts and theorems in conformal geometry. Here we briefly review the basic concepts. Detailed treatments can be found in [41, 17, 42].

3.1. Riemann Surface

Riemann Surface. Riemann surface theory generalizes the complex analysis to the surface setting. Given a complex function $f : \mathbb{C} \to \mathbb{C}$, $f : x + iy \mapsto u(x, y) + iv(x, y)$, if f satisfies the Cauchy-Riemann equation

$$u_x = v_y, u_y = -v_x$$

then f is a *holomorphic function.* If f is invertible, and f^{-1} is also holomorphic, then f is a *bi-holomorphic function.* A two dimensional manifold is called a *surface.* A surface with a complex atlas $\mathcal{A}$, such that all chart transition functions are bi-holomorphic, then it is called a *Riemann surface*, the atlas $\mathcal{A}$ is called a *complex structure.*

Holomorphic Quadratic Differential.

Definition 3.1 (Holomorphic Quadratic Differentials)**.** *Suppose S is a Riemann surface. Let Φ be a complex differential form, such that on each local chart with the local complex parameter $\{z_\alpha\}$,*

$$\Phi = \varphi_\alpha(z_\alpha)dz_\alpha^2,$$

where $\varphi_\alpha(z_\alpha)$ is a holomorphic function.

A holomorphic quadratic differentials on a genus zero closed surface must be 0. On a genus one closed surface, any holomorphic quadratic differential must be the square of a holomorphic 1-form. According to Riemann-Roch theorem,

the dimension of the linear space of all holomorphic quadratic differentials is $3g-3$ complex dimensional, where the genus $g>1$.

A point $z_i \in S$ is called a *zero* of Φ, if $\varphi(z_i)$ vanishes. A holomorphic quadratic differential has $4g-4$ zeros, as shown in Fig. 9. For any point away from zero, we can define a local coordinates

$$\zeta(p) := \int^p \sqrt{\varphi(z)}dz. \tag{1}$$

which is the so-called *natural coordinates* induced by Φ. The curves with constant real natural coordinates are called the *vertical trajectories*, with constant imaginary natural coordinates *horizontal trajectories*. The trajectories through the zeros are called the *critical trajectories*.

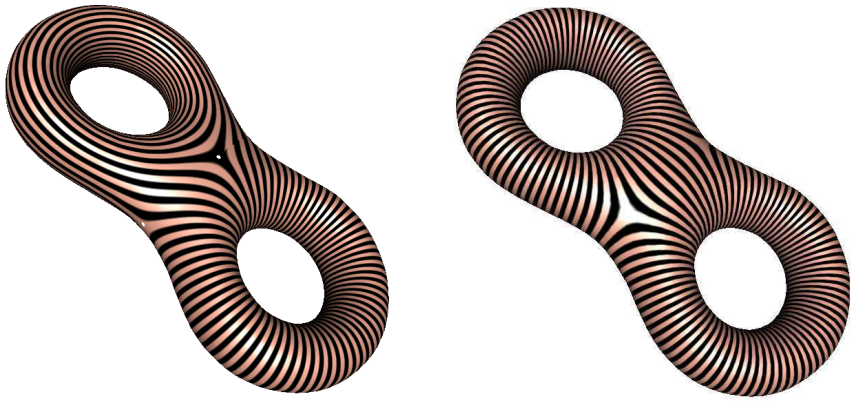

Figure 9: Holomorphic quadratic forms on a genus two surface.

As shown in Fig. 10, the bunny surface is of genus zero. we slice the surface at the ear tips, and the bottom. The red and blue curves are horizontal and vertical trajectories of a holomorphic differential on the surface.

Definition 3.2 (Strebel[42])**.** *Given a holomorphic quadratic differential Φ on a Riemann surface S, if all of its horizontal trajectories are finite, then Φ is called a Strebel differential.*

A holomorphic quadratic differential Φ is Strebel, if and only if its critical horizontal trajectories form a finite graph [42]. As shown in Fig. 11, the hori-

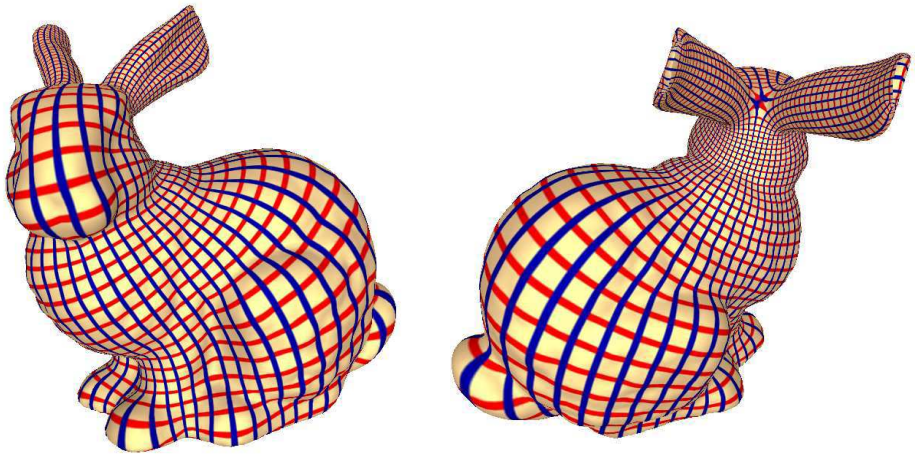

Figure 10: The horizontal (red) and vertical (blue) trajectories of a holomorphic 1-form on a genus zero surface with three boundaries.

(a) Non-Strebel (b) Strebel

Figure 11: A non-Strebel (a) and a Strebel differential (b) on a genus two surface. The Strebel differential has finite horizontal trajectories.

290 zontal trajectories of a holomorphic differential may be infinite spirals as in the left frame, or finite loops as in the right frame.

Conformal Mapping and Teichmüller Space. Suppose $(\mathcal{S}, \{z_\alpha\})$ and $(\mathcal{T}, \{w_\beta\})$ are two Riemann surfaces, $\varphi : \mathcal{S} \to \mathcal{T}$ is a smooth mapping between them. If

every local representation of φ, $z_\alpha \mapsto w_\beta$ is holomorphic, then the mapping is called a *conformal mapping*. If the local representation is biholomorphic, then the two Riemann surfaces are *conformal equivalent*.

Figure 12 demonstrates a conformal mapping from a human facial surface onto the planar unit disk. A conformal mapping maps infinitesimal circles to infinitesimal circles, this shows that the tangential map of a conformal mapping is a scaling map, therefore a conformal mapping preserves angles.

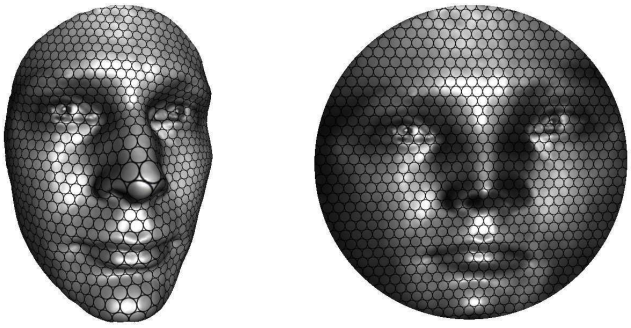

Figure 12: A conformal mapping from a human face surface onto the unit planar disk.

Suppose S is an oriented topological surface, with two conformal structures $\{z_\alpha\}$ and $\{w_\beta\}$, if there exists a bi-holomorphic map $\varphi : (S, \{z_\alpha\}) \to (S, \{w_\beta\})$ and φ is homotopic to the identity map of S, then we say $(S, \{z_\alpha\})$ and $(S, \{w_\beta\})$ are *Tecihmüller equivalent*. All the Teichmüller equivalence classes form a space, which is called the *Teichmüller space* of S.

Conformal Module. Suppose Riemann surface S is a topological annulus, namely a genus zero surface with two boundaries, then there exists a conformal mapping from S to a canonical planar annulus. The inner and outer circles are with radii r and R respectively. Then the *conformal module* of the surface is defined as

$$\mathrm{Mod}(S) = \frac{1}{2\pi} \log \frac{R}{r}. \tag{2}$$

Equivalently, the topological annulus S can be conformally mapped to a canonical cylinder C. The bottom circle of C is with radius 1 and the height is

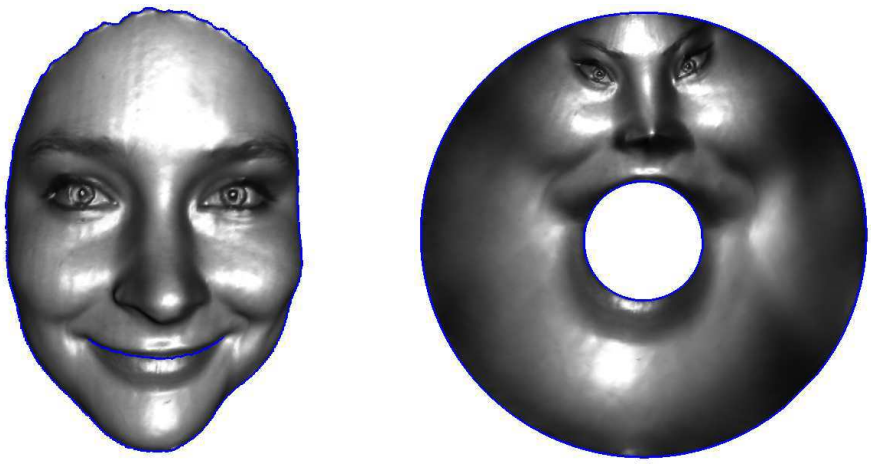

(a) a human facial surface with a slit

(b) a planar annulus

Figure 13: The human facial surface is sliced along the mouth to become a topological annulus (a). The faical surface is conformally mapped to a planar annulus (b). The conformal module of the topological annulus is given by the ratio between the outer and inner radii.

$2\pi\text{Mod}(S)$. There exists a conformal mapping between two topological annuli, if and only if they share the same conformal module.

4. From Quadrilateral Mesh to Strebel Differential

4.1. Colorable Quadrilateral Surface Mesh

Suppose S is a Riemann surface, a *quadrilateral mesh* of S is a geometric *cell decomposition*, such that each cell is topological quadrilateral. More rigorously, we can define a quadrilateral mesh as a geometric *cell complex* composed of 0-dimensional nodes, 1-dimensional edges and 2-dimensional quadrilaterals, such that

1. Each edge contains two distinct nodes;
2. Each face is contained in at least one higher-dimensional face, i.e. each node is in an edge, each edge is in a quadrilateral.
3. Every edge is in exactly two distinct quadrilaterals.

4. Each quadrilateral is bounded by a cycle of four distinct edges.
5. Two nodes have at most one edge between them.
6. Two quadrilaterals share at most one edge.

Suppose $\mathcal{M}$ is a three dimensional manifold, a *hexahedral mesh* of $\mathcal{M}$ is a geometric *cell decomposition*, such that each cell is a topological hexahedron. A more rigorous definition can be found in [10].

Definition 4.1 (Colorable Quad Mesh)**.** *Suppose Q is a quadrilateral mesh on a surface S, if there is a coloring scheme $\iota : E \to \{red, blue\}$, which colors each edge either red or blue, such that each quadrilateral face includes two opposite red edges and two opposite blue edges, then Q is called a colorable (red-blue) quadrilateral mesh.*

Two quadrilateral meshes for a multi-connected planar domain are shown in Figure 4. The domain is a topological disk with two inner holes. The left quad-mesh is with a color scheme. The right quad mesh is not colorable. The black edge in the middle can be colored neither red nor blue.

Lemma 4.2. *Suppose S is an oriented closed surface, $\mathcal{Q}$ is a quadrilateral mesh on S. $\mathcal{Q}$ is colorable if and only if the valences of all vertices are even.*

Proof. Necessary Condition Suppose v is a vertex of the quad mesh $\mathcal{Q}$, the edges adjacent to v are sorted counter-clock-wisely with respect to the orientation of the surface, denoted as $\{e_0, e_1, \cdots, e_k\}$. Because $\mathcal{Q}$ is colorable, therefore, the colors of the edges are either $\{red, blue, \cdots, red, blue\}$ or $\{blue, red, \cdots, blue, red\}$, hence the number of edges are even. Because v is an arbitrary vertex of $\mathcal{Q}$, the valence of every vertex is even.

Sufficient Condition Consider each vertex v in $\mathcal{Q}$, if the valence of v is 4, then v is a regular vertex, otherwise, v is a singular vertex. Let the set of all singular vertices be

$$P := \{v \in \mathcal{Q} | \deg(v) \neq 4\}.$$

Let

$$\mathcal{R} := S \setminus P$$

be the punctured surface with all singularities removed, each quadrilateral face be the canonical planar square, then the punctured surface is with a flat metric $\mathbf{g}$, denoted as $(\mathcal{R}, \mathbf{g})$. Consider the universal covering space of the punctured flat surface $\pi : \tilde{\mathcal{R}} \to (\mathcal{R}, \mathbf{g})$. Then all the deck transformations of $(\tilde{\mathcal{R}}, \pi^*\mathbf{g})$ must be Euclidean rigid motions of the plane. Let $v \in P$ be a singular vertex, γ be a small loop surrounding v, then the deck transformation corresponding to $[\gamma]$ is a rotation of $k\pi$, where k is an integer. All the deck transformations are with form $(x, y) \mapsto \pm(x, y) + (m, n)$. Let e be an edge in $\mathcal{Q}$, its orbit in the covering space is

$$\pi^{-1}(e) = \{\cdots, \tilde{e}_i, \cdots, \tilde{e}_j, \cdots\},$$

where $\tilde{e}_i$ and $\tilde{e}_j$ differs by a deck transformation, therefore they are parallel to each other.

We isometrically immerse $(\tilde{\mathcal{R}}, \pi^*\mathbf{g})$ in the plane, such that each edge is either horizontal or vertical, we color the horizontal edges red, and vertical edges blue. Then for each edge $e \in \mathcal{Q}$, all its preimages are in the same color. Then we color e by the same color of its orbit. This gives $\mathcal{Q}$ a consistent color scheme. □

Lemma 4.3. *Suppose S is an oriented closed surface, $\mathcal{Q}$ is a quadrilateral mesh on S. If $\mathcal{Q}$ is colorable, then the dual curve arrangement $\tilde{\mathcal{Q}}$ of $\mathcal{Q}$ consists of finite loops without self-intersections.*

Proof. Suppose the quad mesh $\mathcal{Q}$ is with a consistent color scheme. Consider an arbitrary dual curve γ of $\mathcal{Q}$. Then by definition, γ only intersects either red edges, or blue edges. Assume γ intersects itself at a point p, p is inside a quadrilateral face f, then γ transverses both the red edges and blue edges of f, contradiction. Hence γ has no self-intersection, namely the dual curve arrangement of $\mathcal{Q}$ consists of finite loops without self-intersection. □

4.2. Finite Measured Foliation

Definition 4.4 (Measured Foliation)**.** *Let S be a compact Riemann surface of genus $g > 1$. A C^k measured foliation on S with singularities $z_1, \ldots, z_l$ of order $k_1, \ldots, k_l$ respectively is given by an open covering $\{U_i\}$ of $S - \{z_1, \ldots, z_l\}$*

Figure 14: A finite measured foliation on a genus three surface.

and open sets $V_1, \ldots, V_l$ *around* $z_1, \ldots, z_l$ *respectively along with* C^k *real valued functions* v_i *defined on* U_i *s.t.*

1. $|dv_i| = |dv_j|$ *on* $U_i \cap U_j$
2. $|dv_i| = |Im(z - z_j)^{k_j/2} dz|$ *on* $U_i \cap V_j$.

The kernels $\ker dv_i$ *define a* C^{k-1} *line field on* S *which integrates to give a foliation* $\mathcal{F}$ *on* $S - \{z_1, \ldots, z_l\}$*, with* $k_j + 2$ *pronged singularity at* z_j*. Moreover, given an arc* $\gamma \subset S$*, we have a well-defined measure* $\mu(\gamma)$ *given by*

$$\mu(\gamma) = |\int_\gamma dv|$$

where $|dv|$ *is defined by* $|dv|_{U_i} = |dv_i|$.

If each leaf of the measured foliation $(\mathcal{F}, \mu)$ is a finite loop, then $\mathcal{F}$ is called a *finite measured foliation.*

Two measured foliations $(\mathcal{F}, \mu)$ and $(\mathcal{G}, \nu)$ are said to be equivalent if after some Whitehead moves on $\mathcal{F}$ and $\mathcal{G}$, there is a self-homeomorphism of S which takes $\mathcal{F}$ to $\mathcal{G}$, and μ to ν. Here a Whitehead move is the transformation of one foliation to another by collapsing a finite arc of a leaf between two singularities, or the inverse procedure, as shown in Figure 15.

Lemma 4.5. *Suppose* S *is a closed oriented surface,* $\mathcal{Q}$ *is a colorable quadrilateral mesh of the surface, then* $\mathcal{Q}$ *induces two finite measured foliations.*

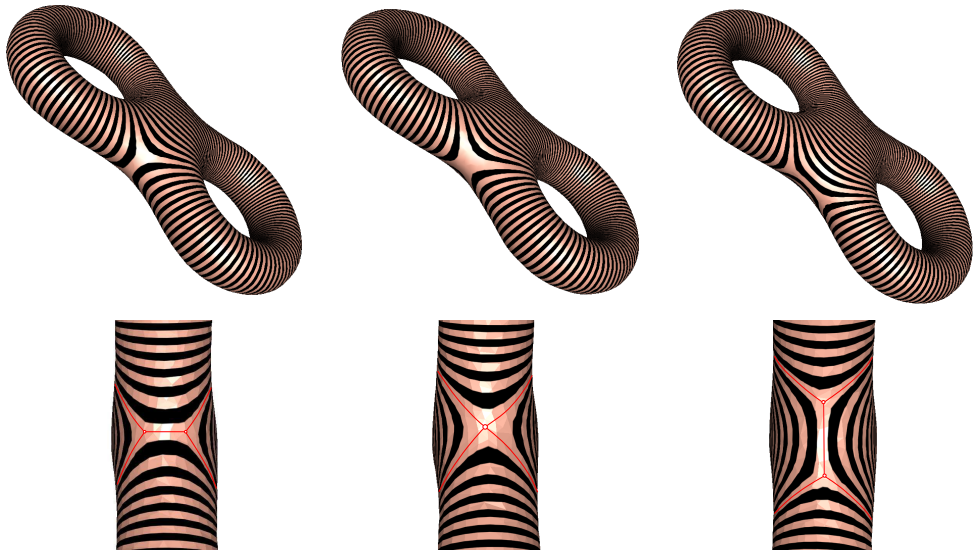

Figure 15: Equivalent measured foliations and Whitehead moves.

Proof. We remove the vertices of $\mathcal{Q}$ from S, whose valences are not equal to 4, and obtain a punctured surface $\mathcal{R}$. Assume each quad-face is a canonical unit square, then this defines a flat metric on $\mathcal{R}$. Let $\pi : \tilde{\mathcal{R}} \to \mathcal{R}$ be the universal covering space of the punctured surface, the universal covering space is equipped with the pull-back flat metric and immersed on the Euclidean plane. Because all the singularities are with even valences, then all the deck transformations have the form $z \mapsto \pm z + a$. We can adjust the immersion, such that the red edges of one quad-face are aligned with the real axis, and the blue edges with the imaginary axis. This gives two local foliations $(y = \text{const}, |dy|)$ and $(x = \text{const}, |dx|)$. Because the holonomy consists of rotations by $k\pi$, where k is an integers, the local foliations can be extended to cover the whole surface. □

In the following, we call the foliations aligned with the red edges as the *horizontal foliation* induced by $\mathcal{Q}$, the one aligned with the blue edges as the *vertical foliation* induced by $\mathcal{Q}$.

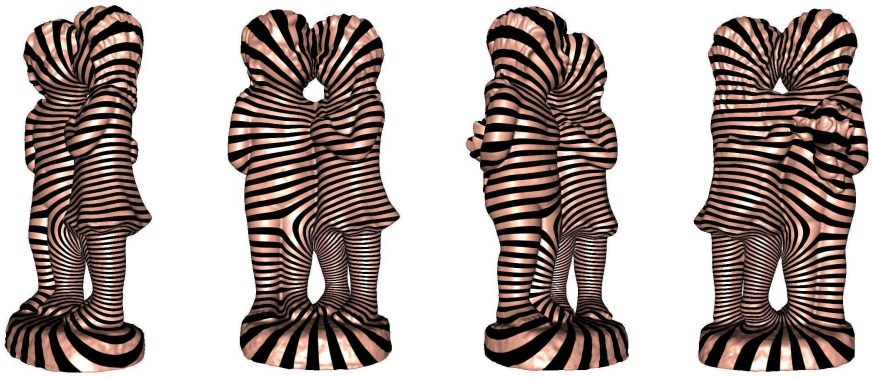

Figure 16: Holomorphic quadratic differentials on a genus three surface.

4.3. Strebel Differential

Given a holomorhic quadratic differential Φ on a Riemman surface S, it defines a measured foliation in the following way: Φ induces the natural coordinates ζ, the local measured foliations are given by

$$(\{\mathrm{Im}\zeta = \mathrm{const}\}, |d\mathrm{Im}\zeta|), \tag{3}$$

then piece together to form a measured foliation known as the *horizontal measured foliation* of Φ. Similarly, the vertical measured foliation of Φ is given by

$$(\{\mathrm{Re}\zeta = \mathrm{const}\}, |d\mathrm{Re}\zeta|). \tag{4}$$

Hubbard and Masure proved the following fundamental theorem connecting measured foliation and holomorphic quadratic differentials.

Theorem 4.6 (Hubbard-Masur [43])**.** *If $(\mathcal{F}, \mu)$ is a measured foliation on a compact Riemann surface S, then there is a unique holomorphic quadratic differential Φ on S whose horizontal foliation is equivalent to $(\mathcal{F}, \mu)$.*

Corollary 4.7. *Suppose S is a closed compact Riemann surface, $\mathcal{Q}$ is a colorable quadrilateral mesh, then there exists a unique Strebel differential Φ, the horizontal measured foliation of Φ is equivalent to the horizontal foliation induced by $\mathcal{Q}$.*

Proof. By lemma 4.5, the colorable quad-mesh $\mathcal{Q}$ induces a finite measurable foliation $(\mathcal{F}_\mathcal{Q}, \mu_\mathcal{Q})$, the horizontal foliation induced by $\mathcal{Q}$. By theorem 4.6, there exists a unique holomorphic quadratic differential Φ, whose horizontal measured foliation is equivalent to the finite measured foliation $(\mathcal{F}_\mathcal{Q}, \mu_\mathcal{Q})$. Furthermore, due to the finiteness of $(\mathcal{F}_\mathcal{Q}, \mu_\mathcal{Q})$, Φ is a Strebel differential. □

Similarly, it can be shown there is a unique Strebel differential, whose horizontal foliation is equivalent to the vertical foliation induced by $\mathcal{Q}$.

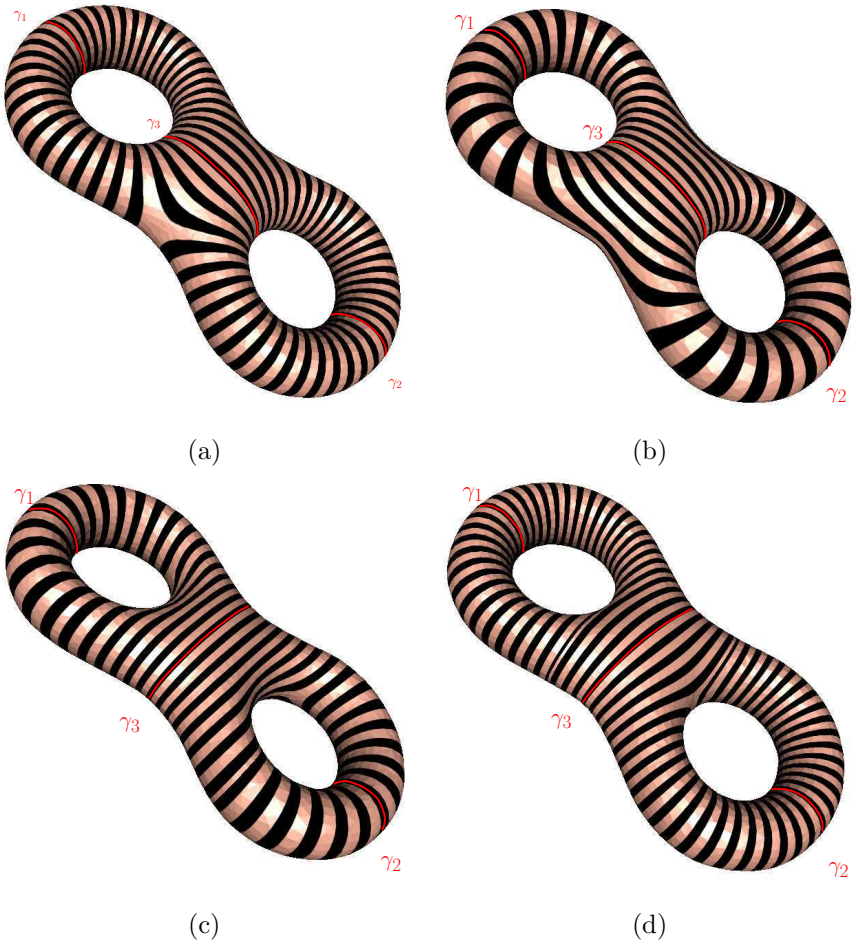

Figure 17: Holomorphic quadratic differentials on the genus two surface.

5. From Strebel Differential to Quadrilateral Mesh

In this section, we prove that each Strebel differential induces a colorable quadrilateral mesh.

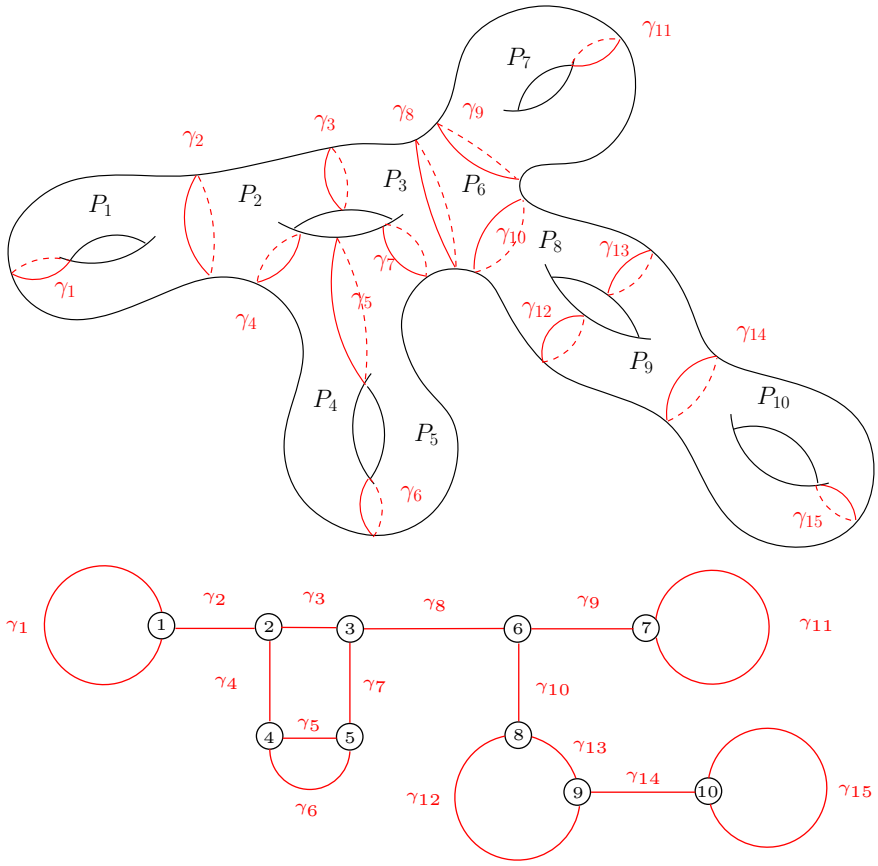

Figure 18: Holomorphic quadratic differentials on the genus two surface.

5.1. Pants Decomposition Graph

Given a genus $g > 1$ closed surface S, we select $3g - 3$ disjoint simple loops, $\{\gamma_1, \gamma_2, \cdots, \gamma_{3g-3}\}$, which segment the surface into $2g - 2$ pairs of pants, $\{P_1, P_2, \cdots, P_{2g-2}\}$. Each pair of pants is a genus 0 surface with 3 boundary loops. This is called a *pants decomposition* of the surface. A pants decomposition can be represented as a graph G, each pair of pants is represented as a node,

each simple loop is denoted by an edge. Suppose the simple loop γ_i connecting two pairs of pants P_j, P_k, then the arc of γ_i connects nodes of P_j and P_k. In the following discussion, we call G as the *pants decomposition graph*. Figure 18 shows one example.

Definition 5.1 (Pants decomposition Graph)**.** *Suppose G is a graph, $g > 1$ is a positive integer, such that there are $2g-2$ nodes, $3g-3$ edges, the valence of each node is 3. Then we call G a pants-decomposition graph, g the genus of the graph.*

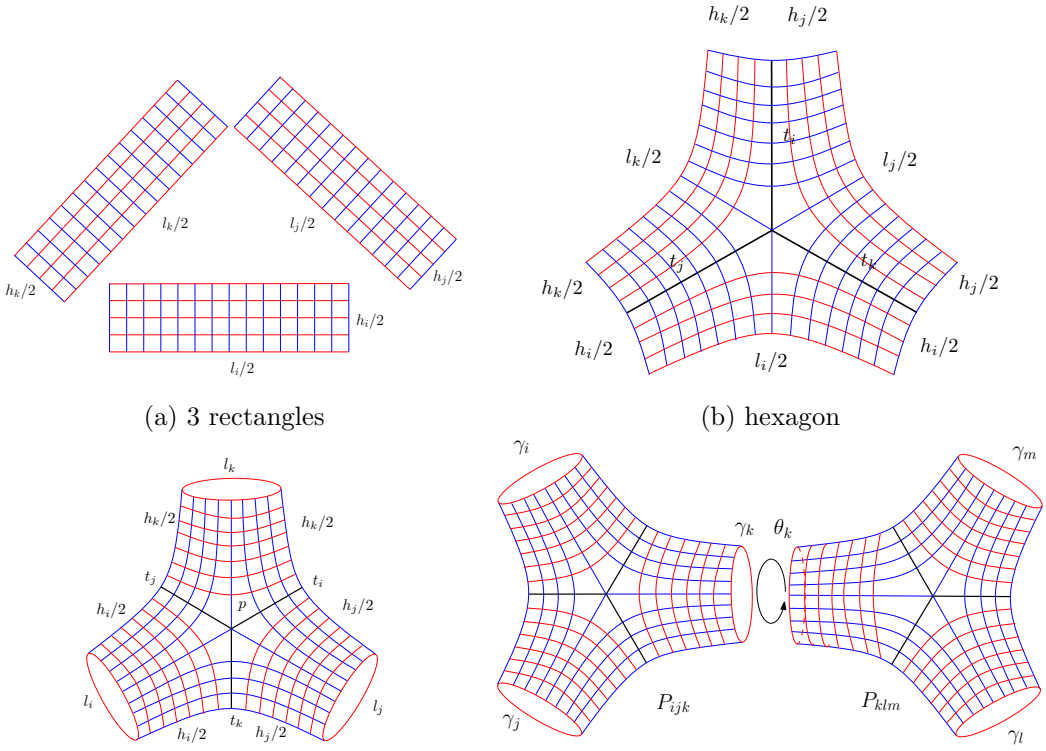

(a) 3 rectangles

(b) hexagon

(c) a pair of pants

(d) gluing two pairs of pants

Figure 19: Flat cylindric surface model of $(S, |\Phi|)$.

5.2. Existence of Strebel Differential

All the Strebel quadratic differentials are dense in the space of all holomorphic quadratic differentials. Given a holomorphic quadratic differential Φ,

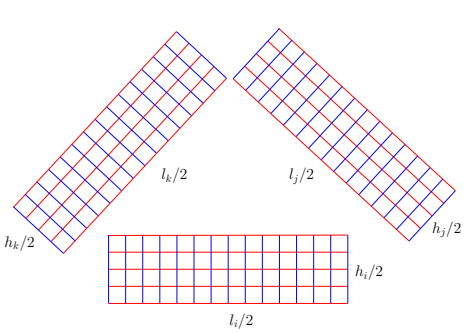

(a) 3 rectangles $l_j + l_k > l_i$

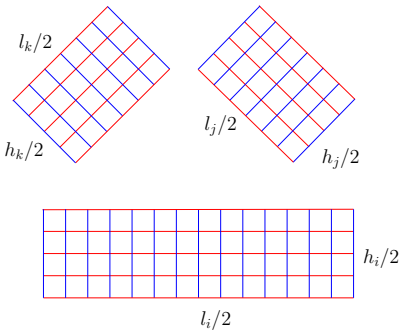

(b) 3 rectangles $l_j + l_k < l_i$

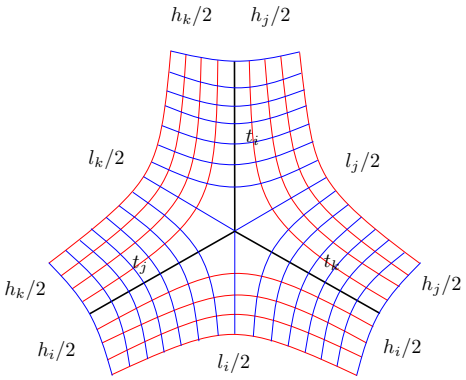

(c) a hexagon

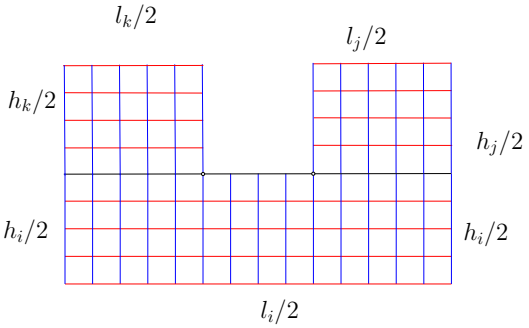

(d) an octagon

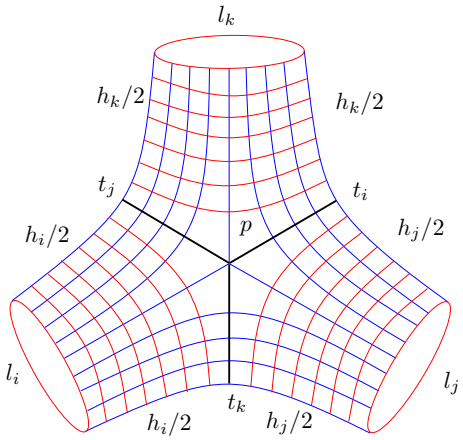

(e) a pair of pants (type I)

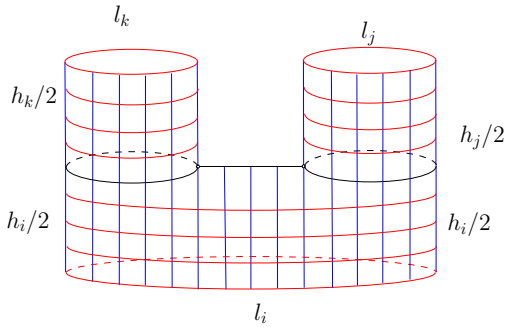

(f) a pair of pants (type II)

Figure 20: Flat cylindric surface model of $(S, |\Phi|)$.

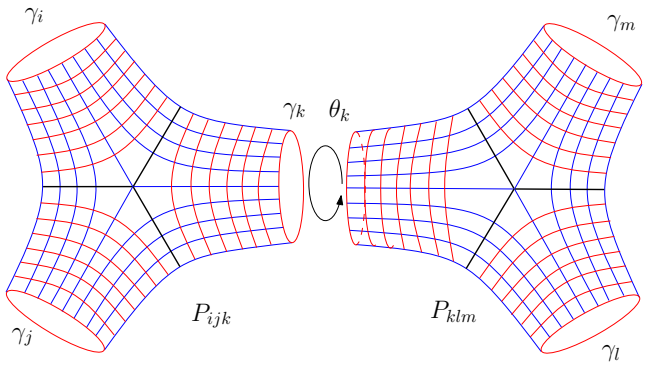

Figure 21: The twisting angle when gluing two pair of pants.

the natural coordinates in Eqn. 1 induces a flat metric with cone singularities, which is denoted as $|\Phi|$. Hubbard and Masur proved the following existence of a Strebel differential with prescribed type and heights.

Definition 5.2 (Admissible Curve System)**.** *On a genus g surface S, a set of non-intersecting simple loops $\Gamma = \{\gamma_1, \gamma_2, \cdots, \gamma_n\}$, where $n \leq 3g-3$ is called an* admissible curve system.

Theorem 5.3 (Hubbard and Masur [43])**.** *Given non-intersecting simple loops $\Gamma = \{\gamma_1, \gamma_2, \cdots, \gamma_{3g-3}\}$, and positive numbers $\{h_1, h_2, \cdots, h_{3g-3}\}$, there exists a unique holomorphic quadratic differential Φ, satisfying the following :*

1. *The critical graph of Φ partitions the surface into $3g-3$ cylinders, $\{C_1, C_2, \cdots, C_{3g-3}\}$, such that γ_k is the generator of C_k,*
2. *The height of each cylinder $(C_k, |\Phi|)$ equals to h_k, $k = 1, 2, \cdots, 3g-3$.*

The geometric interpretation of Hubbard and Masur's theorem is as follows: given a holomorphic quadratic differential Φ, the natural coordinates ζ in Eqn. 1 induces a flat metric at the regular points, and cone angles $-\pi$ at the zeros. Each cylinder C_k becomes a canonical flat cylinder under $|\Phi|$, whose height is h_k. Therefore, Hubbard and Masur's theorem allows one to specify the type of Φ and the height of each cylinder C_k.

As shown in Fig. 17, given three disjoint simple loops $\{\gamma_1, \gamma_2, \gamma_3\}$ and three

height parameters $\{h_1, h_2, h_3\}$, the corresponding Strebel differentials are illustrated by their horizontal trajectories. Each pair (a) and (b), (c) and (d) share the same admissible curves, but different height parameters.

5.3. Poly-Cylinder Surface

Given a pants decomposition graph G, we associate each arc γ_k with a positive number $h_k > 0$, such that there exists a Strebel differential Φ, the critical trajectories of Φ segment the surface into cylinders $\{C_k\}$, the fundamental group generator of C_k is γ_k. The height of C_k under the metric induced by $|\Phi|$ is h_k, assume the circumference of C_k is l_k. The surface $(S, |\Phi|)$ can be treated as constructed in the following way: we use P_{ijk} to denote the pair of pants with three boundary loops $\gamma_i, \gamma_j, \gamma_k$.

Step 1. For each boundary loop γ_i, we construct a rectangle R_i with width $l_i/2$ and height $h_i/2$, as shown in Fig.20 frame (a); the horizontal iso-parametric curves are red, the vertical iso-parametric curves are blue.

Step 2. If $\{l_i, l_j, l_k\}$ satisfy the triangle inequality, then three rectangles R_i, R_j and R_k are glued together to form a flat hexagon with cone singularity p as shown in frame (c), where

$$t_i = R_j \cap R_k,\ t_j = R_i \cap R_k,\ t_k = R_i \cap R_j.$$

The lengths are given by

$$t_i = \frac{l_j + l_k - l_i}{4}, t_j = \frac{l_k + l_i - l_j}{4}, t_k = \frac{l_i + l_j - l_k}{4}.$$

If $\{l_i, l_j, l_k\}$ don't satisfy the triangle inequality, $l_j + l_k < l_i$, then three rectangles R_i, R_j and R_k are glued together to form a flat octagon as shown in frame (d).

Step 3. Glue two copies of the hexagons in (c) along the three blue boundary segments to form a pairs of pants P_{ijk} in (e). Similarly, glue two copies of the

octagons in (d) along the 4 blue boundary segments to form a pairs of pants P_{ijk} in (f). The red and blue curves are horizontal and vertical trajectories of Φ respectively. Two cone singularises are the two zeros of Φ. The black curves $\{t_i, t_j, t_k\}$ form the critical horizontal trajectory in (e) and (f).

Step 4. For each node in the pants decomposition graph G, we construct a pair of pants. For each edge γ_k in the graph, we connect two pairs of pants P_{ijk} and P_{klm} along the common boundary loop γ_k by twisting P_{klm} by an angle θ_k.

We call the obtained surface as *poly-cylinder surface*, in fact it is isometric to $(S, |\Phi|)$.

Definition 5.4 (Poly-cylinder surface)**.** *Given a pants-decomposition graph $G = \langle V, E\rangle$, a cylinder height function $h : E \to \mathbb{R}^+$, a cylinder circumference function $l : E \to \mathbb{R}^+$, a twisting angle function $\theta : E \to \mathbb{R}$, the surface constructed as above is called a poly-cylinder surface, denoted as $\mathcal{S} := (G, h, l, \theta)$.*

The above argument leads to the following lemma.

Lemma 5.5. *Suppose S is a closed Riemannian surface, Φ is a Strebel differential, then it induces a poly-cylinder surface (G, h, l, θ).*

Inversely, if we fix the pants decomposition graph G, and the cylinder height function h, vary the circumference function l and the twisting angle function θ, then the poly-cylinder surface (G, h, l, θ) can cover the Teichmüller space.

Theorem 5.6 (Teichmüller Coordinates[44])**.** *Given a topological surface S, fixing a pants decomposition graph G, and the cylinder height function h, vary the circumference function l and the twisting angle function θ, then the poly-cylinder surface (G, h, l, θ) can cover a neighborhood of the Teichmüller space of S.*

5.4. Quadrilateral Mesh Generation

Lemma 5.7. *Suppose Φ is a Strebel differential on a compact Riemann surface S with genus greater than 0, then Φ induces a colorable (red-blue) quadrilateral*

mesh $\mathcal{Q}_\Phi$ *of* S.

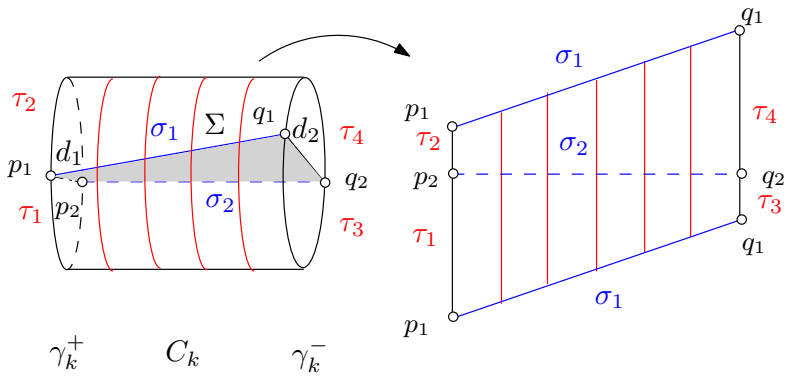

Figure 22: Quadrilateral meshing a cylinder.

Proof. By Lemma 5.5, the Strebel differential Φ induces poly-cylinder surface. Suppose P_{ijk} is a pair of pants, such that l_i, l_j, l_k doesn't satisfy the triangle inequality, like the situation of Fig. 20 frame (f), then by the Whitehead move, we can deform the critical graph as that in frame (e). The surface is segmented into cylinders by the modified critical graph, each cylinder C_k has two boundaries γ_k^+ and γ_k^-, each boundary traverses the singularities twice, as shown in Fig. 22, p_1, p_2 are on γ_k^+ and q_1, q_2 are on γ_k^-, then we draw two curves on C_k, connecting p_1 and q_1, p_2 and q_2 respectively. This form a quadrilateral mesh $\mathcal{Q}$ of the surface. All the vertices are the zeros of Φ, the valence of each zero is 6. By Lemma 4.2, $\mathcal{Q}$ is colorable. The edges on the critical graph are in red, the edges connecting p_i to q_i in each cylinder are in blue. □

Furthermore, in $\mathcal{Q}_\Phi$, we use τ_i to represent the edges on the critical graph of Φ, and σ_j the edges connecting zeros on each cylinder. The symbols $\{C_k, \sigma_i, \tau_j\}$ are shown in Fig. 22.

6. Main Theorem

By previous discussion, we are ready to prove the main theorem of the current work:

Theorem 6.1 (Trinity)**.** *Suppose S is a compact Riemann surface with genus greater than one. Given a colorable quadrilateral mesh $\mathcal{Q}$, there is a finite measured foliation $(\mathcal{F}_\mathcal{Q}, \mu_\mathcal{Q})$ induced by $\mathcal{Q}$, and there exits a unique Strebel different Φ, such that the horizontal measured foliation induced by Φ, $(\mathcal{F}_\Phi, \mu_\Phi)$ is equivalent to $(\mathcal{F}_\mathcal{Q}, \mu_\mathcal{Q})$.*

Inversely, given a Strebel differential Φ, it is associated with a finite measured foliation $(\mathcal{F}_\Phi, \mu_\Phi)$, and induces a colorable quadrilateral mesh $\mathcal{Q}$.

Proof. Given a colorable $\mathcal{Q}$ on S, by lemma 4.5, the horizontal foliation $(\mathcal{F}_\mathcal{Q}, \mu_\mathcal{Q})$ induced by $\mathcal{Q}$ is a finite measured foliation. Then by corollary 4.7, there exits a unique Strebel differential Φ, such that the horizontal measured foliation induced by Φ, $(\mathcal{F}_\Phi, \mu_\Phi)$ is equivalent to $(\mathcal{F}_\mathcal{Q}, \mu_\mathcal{Q})$.

Inversely, given a Strebel differential Φ, it is associated with a finite measured foliation $(\mathcal{F}_\Phi, \mu_\Phi)$ given by $(\{\mathrm{Im}\zeta = \mathrm{const}\}, |d\mathrm{Im}\zeta|)$, where ζ is the natural coordinates induced by Φ as described in Eqn.1. Then by lemma 5.7, Φ induces a colorable quad-mesh of S. □

We can systematically generate Strebel differentials on a compact Riemann surface, each Strebel differential induces a colorable quad-mesh, then in turn a hexahedral mesh of the interior solid.

We can show that a Strebel differential induces a hexahedral mesh. A surface S embedded in $\mathbb{R}^3$, separates $\mathbb{R}^3$ into two connected components, the enclosed volume $\mathcal{I}$ and the outside space $\mathcal{O}$. A *handle-body* can be defined as an orientable 3-manifold with boundary containing pairwise disjoint, properly embedded 2-discs such that the manifold resulting from cutting along the discs is a 3-ball. In other words, a handle-body can be constructed by gluing a finite number of 1-handles (solid cylinders) to a 3-ball. In the following, we assume $\mathcal{I}$ is a handle body.

Theorem 6.2. *Suppose S is a compact Riemann surface with genus $g > 1$ embedded in $\mathbb{R}^3$, the interior solid $\mathcal{I}$ is a handle-body, then there exists a Strebel*

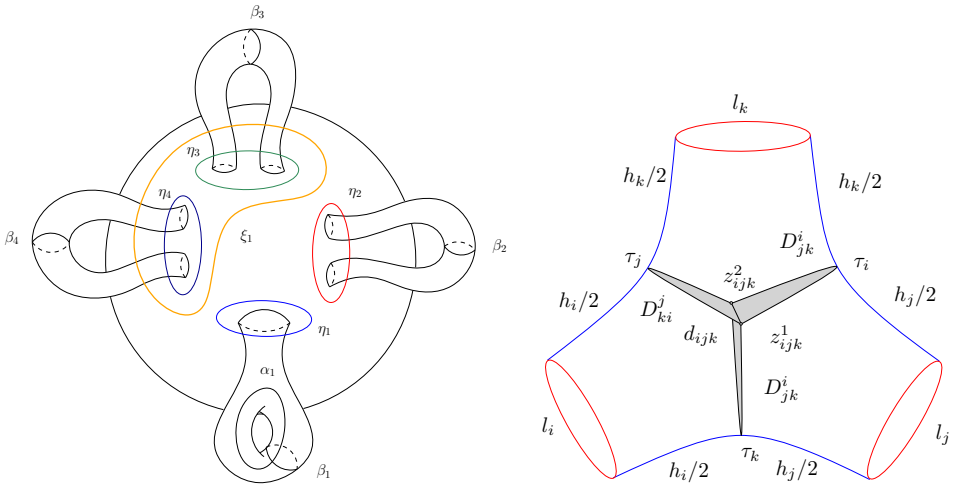

(a) Admissible curve system (b) Cutting half-disks

Figure 23: Construction of the admissible curve system, and the cutting half-disks.

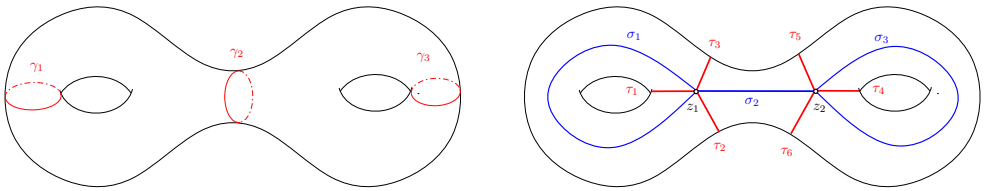

(a) Admissible curve system $\Gamma = \{\gamma_1, \gamma_2, \gamma_3\}$ (b) Colorable quad-mesh $\mathcal{Q}_\Phi$

Figure 24: Given an admissible curve system Γ (a) and the height $\mathbf{h}$, there exists a consistent Strebel differential Φ, which induces a colorable qaud-mesh in (b). The zeros are z_1, z_2, the critical graph is formed by $\{\tau_1, \tau_2, \tau_3, \tau_4, \tau_5, \tau_6\}$ The vertical STC chords of $\mathcal{Q}_\phi$ is shown as $\{\sigma_1, \sigma_2, \sigma_3\}$.

differential Φ, such that Φ induces a colorable quad-mesh $\mathcal{Q}_\Phi$, $\mathcal{Q}_\Phi$ can be extended to a hexahedral mesh of the enclosed volume $\mathcal{I}$.

Furthermore, the hex-mesh has tensor product structure except at $2g-2$ singular curves.

Proof. The proof is constructive, which leads to a computational algorithm directly.

Step 1. Construct the pants decomposition graph

As shown in Fig. 23 frame (a), the handle-body has $g > 1$ handles, the cutting disks are $\{D_1, D_2, \cdots, D_g\}$, whose boundaries are

$$\{\beta_1, \beta_2, \cdots, \beta_g\}, \beta_i = \partial D_i, i = 1, 2, \cdots, g.$$

As shown in Fig. 23 frame (a), assume each handle has another generator α_i, then we obtain loops

$$\{\eta_1, \eta_2, \cdots, \eta_g\}, \eta_i = \alpha_i \beta_i \alpha_i^{-1} \beta_i^{-1}, i = 1, 2, \cdots, g.$$

The k-th handle can be cut off from S by slicing along η_k. After removing g handles, the left part of S is a denoted as $\mathcal{C}$. $\mathcal{C}$ is a genus 0 surface with g boundary loops,

$$\partial \mathcal{C} = \eta_1 \cup \eta_2, \cdots, \cup \eta_g.$$

If g equals to 2, η_1 and η_2 coincide, $\{\beta_1, \beta_2, \eta_1\}$ form an admissible curve system. If g equals 3, $\{\beta_1, \beta_2, \beta_3, \eta_1, \eta_2, \eta_3\}$ form an admissible curve system. Otherwise, we find one loop ξ_1 on $\mathcal{C}$ circling around η_1 and η_2, cut the surface $\mathcal{C}$ along ξ_1 to remove η_1, η_2. This operation removes two boundary loops from $\mathcal{C}$ and adds back one boundary loop, the total number of boundary loops is reduced by one. We repeat this procedure, each time find a loop ξ_i surrounding two boundary loops on $\mathcal{C}$, and cut the surface along ξ_i to reduce the number of boundary loops by one, eventually $\mathcal{C}$ has only 3 boundary loops, then we stop. In total, we introduce $g - 3$ such kind of loops

$$\{\xi_1, \xi_2, \cdots, \xi_{g-3}\}.$$

Now we have obtained an admissible curve system

$$\Gamma = \bigcup_{i=1}^{g} \{\beta_i\} \bigcup_{j=1}^{g} \{\eta_j\} \bigcup_{k=1}^{3g-3} \{\xi_k\},$$

then construct the pants decomposition graph G_Γ.

Step 2. Construct the Strebel Differential Φ

We set the height parameters $\mathbf{h} = \{h_1, h_2, \cdots, h_{3g-3}\}$, by theorem 5.3 we can find the unique Strebel differential Φ sepcified by $(G_\Gamma, \mathbf{h})$.

Step 3. Solid Cylinder Decomposition

The critical graph segments S into $3g-3$ cylinders $\{C_1, C_2, \cdots, C_{3g-3}\}$, the height of $(C_k, |\Phi|)$ is h_k. The meridian of C_i (the horizontal trajectory of Φ which divides C_i into two equal parts) is denoted as l_i. $\{l_1, l_2, \cdots, l_k\}$ divide the surface S into $2g-2$ pairs of pants.

Fig. 23 frame (b) shows one pair of pants P_{ijk}, $\partial P_{ijk} = l_i \cup l_j \cup l_k$. P_{ijk} contains two zeros of Φ, z^1_{ijk} and z^2_{ijk}, three critical horizontal trajectories τ_i, τ_j and τ_k, which form a connected component of the critical graph of Φ. Inside the enclosed volume $\mathcal{I}$, we can draw a curve segment d_{ijk} connecting the two zeros. This configuration gives three cutting-half-disks inside $\mathcal{I}$, such that

$$\partial D^i_{jk} = \tau_i \cup d_{ijk},\ \partial D^j_{ki} = \tau_j \cup d_{ijk},\ \partial D^k_{ij} = \tau_k \cup d_{ijk},$$

shown as the shadowed regions in Fig. 23 frame (b).

The volume $\mathcal{I}$ is segmented by these cutting half-disks $\{D^k_{ij}\}$ into solid cylinders, each solid cylinder is denoted as T_k, $k = 1, 2, \cdots, 3g-3$.

Step 4. Construct the Hexahedral Mesh

By Lemma 5.7, the Strebel differential Φ induces a colorable quad-mesh $\mathcal{Q}_\Phi$ as shown in Fig. 24 frame (b). The red edges of $\mathcal{Q}_\Phi$ consists of the critical horizontal trajectories of Φ, $\{\tau_i\}$. The blue edges of $\mathcal{Q}_\Phi$ are denoted as $\{\sigma_j\}$. As shown in Fig. 22, inside each solid cylinder T_k, we can construct the surface Σ_k, whose boundaries are the red and blue edges of $\mathcal{Q}_\Phi$. Σ_k divides T_k into two half-solid-cylinders.

If two half-solid-cylinders share the same cutting-half-disk D^k_{ij}, then they are glued together. In this way, all the half-solid-cylinders are glued together, each connected component has a tensor product structure $\mathbb{D} \times \mathbb{S}^1$, which we call *a loop of half-solid-cylinders*. In this way, the volume $\mathcal{I}$ is decomposed into a finite set of loops of half-solid-cylinders.

The hexahdral mesh on each loop of half-solid-cylinders can be constructed easily by "sweeping method", such that the meshing is consistent on the cutting surfaces $\{\Sigma_k\}$, the cutting-half-disks $\{D^k_{ij}\}$ and the singular curves $\{d_{ijk}\}$.

The hexahedral meshes of all loops of half-solid-cylinders are glued together coherently, to form a hexahedral mesh of the entire volume $\mathcal{I}$. The meshing has tensor product structure except at the singular curves d_{ijk}. □

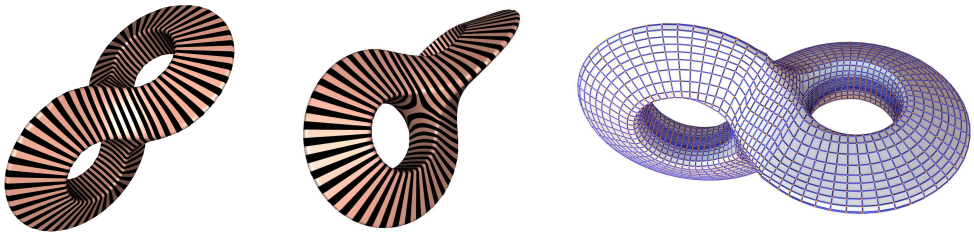

(a) Strebel differential (b) Strebel differential (c) Colorable Quad-mesh

Figure 25: A Strebel differential on a genus two surface (a) and (b) induces a quad meshing (c).

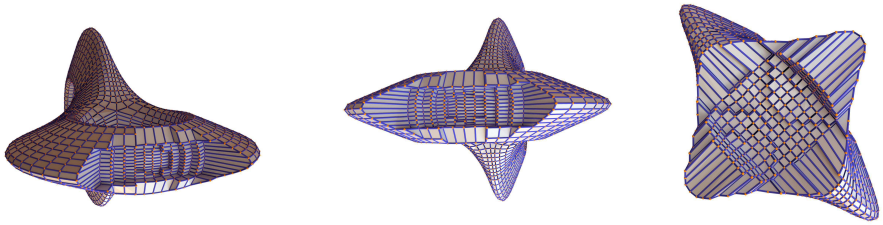

Figure 26: The hexahedral mesh induced by the quadrilateral mesh in Fig. 25.

Fig. 25 and 26 illustrate the process. Frame (a) and (b) of Fig. 25 show the Strebel differential Φ, frame (c) is the induced quad-mesh. Fig. 26 shows the hexahedral mesh of the enclosed volume.

7. Discussion

The current work focuses on the theoretic aspects of the framework of the hexahedral meshing based on foliations, the algorithmic details will be given in the future expositions, including the algorithm of computing the Strebel differential from the pants decomposition graph and the heights, the algorithm of finding the half-cutting disks, the half-solid-cylinder decomposition and so on.

The input is an admissible curve system, which produces a pants-decomposition of the surface. There are ways to automatically generate pants-decomposition, such as the algorithm described in [45]. There are infinite many number of Strebel differentials, hence infinite many ways of hexahedral meshing. It is an intriguing problem to find the way how Strebel differential affects the quality of the hex-mesh, and how to select the optimal solution. This will be one of our future directions.

Current work focuses more on the topological aspect of the algorithm pipeline. The geometric aspects of the algorithms will be discussed in the following expositions, including the ways to choose the pants-decomposition, the height parameters, the cutting half disks, the hex-meshing for each solid cylinder and so on.

Furthermore, the method is based on conformal geometry, the sizes of the hexahedral elements may not be uniform. In near future, we will investigate effective ways to increase the uniformity of the hexahedra, and improve the quality of the hex-meshes.

8. Conclusion

For the purpose of isogeometric analaysis, one of the most common ways is to construct structured hexahedral meshes, which have regular tensor product structure, and fit them by volumetric T-Splines. This theoretic work proposes a novel surface quadrilateral meshing method, colorable quad-mesh, which leads to the structured hexahedral mesh of the enclosed volume for high genus surfaces.

The work proves the equivalence relations among colorable quad-meshes, finite measured foliations and Strebel differentials on the surface. This trinity theorem lays down the theoretic foundation for structured quadrilateral/hexahedral mesh generation, and leads to practical, automatic algorithms.

The work proposes the following algorithm: the user input a set of disjoint, simple loops on a high genus surface, and specify a height parameter for each

loop; a unique Strebel differential is computed with the combinatorial type and the heights prescribed by the user input; the Strebel differential assigns a flat metric on the surface and decompose the surface into cylinders; a colorable quad-mesh is generated by splitting each cylinder into two quadrilaterals, followed by subdivision; the surface cylindrical decomposition is extended inward to induce a solid cylindrical decomposition of the volume; the hexahedral meshing is generated for each volumetric cylinder and then glued together to form a global consistent hex-mesh. The method is rigorous, geometric, automatic and conformal to the geometry.

Current work focuses more on the topological aspect, and the theoretic proofs of the existence of the solution. In near future, we will investigate further the geometric aspects of the framework, and refine the algorithmic pipeline to improve the quality of the hex-meshing.

Acknowledgement

The authors want to thank Dr. Tom Sederberg and Dr. Tom Hughes for introducing the problem to us, and for their consistent encouragements and wholehearted support for years.

References

[1] J. F. Shepherd, C. R. Johnson, Hexahedral mesh generation constraints, Eng. with Comput. 24 (3) (2008) 195–213.

[2] T. Blacker, Meeting the challenge for automated conformal hexahedral meshing, in: 9th International Meshing Roundtable, 2000, pp. 11–20.

[3] P. M. Tuchinsky, B. W. Clark, The hextet hex-dominant automesher: An interim progress report, in: 6th International Meshing Roundtable, 1997, pp. 183–194.

[4] H. Si, Tetgen, a delaunay-based tetrahedral mesh generator, ACM Transactions on Mathematical Software 41 (2) (2015) 11:1–11:36.

[5] T.J.R.Hughes, J. Cottrell, Y. Bazilevs, Isogeometric analysis: Cad, finite elements, nurbs, exact geometry and mesh refinement, Computer Methods in Applied Mechanics and Engineering 194 (2005) 4135–4195.

[6] J. Cottrell, T. Hughes, Y. Bazilevs, Isogeometric Analysis: Toward Integration of CAD and FEA, Wiley, Cichester, U.K., 2009.

[7] T. W. Sederberg, J. Zheng, A. Bakenov, A. H. Nasri, T-splines and t-nurccs, ACM Trans. Graph. 22 (3) (2003) 477–484.

[8] T. Varady, R. Martin, J. Cox, Reverse engineering of geometric models - an introduction, Computer-Aided Design 29 (4) (1997) 255–268.

[9] W. Thurston, Hexahedral decomposition of polyhedra, posting to Sci. Math. (25 October 1993).
URL http://www.ics.uci.edu/~eppstein/gina/Thurston-hexahedra.html

[10] S. A. Mitchell, A characterization of the quadrilateral meshes of a surface which admit a compatible hexahedral mesh of the enclosed volume, in: STACS 96, 13th Annual Symposium on Theoretical Aspects of Computer Science, Grenoble, France, February 22-24, 1996, Proceedings, 1996, pp. 465–476.

[11] D. Eppstein, Linear complexity hexahedral mesh generation., Comput. Geom. 12 (1-2) (1999) 3–16.

[12] J. Erickson, Efficiently hex-meshing things with topology, Discrete & Computational Geometry 52 (3) (2014) 427–449.

[13] M. Müller-Hannemann, Shelling hexahedral complexes for mesh generation., J. Graph Algorithms Appl. 5 (5) (2001) 59–91.

[14] M. Müller-Hannemann, Quadrilateral surface meshes without self-intersecting dual cycles for hexahedral mesh generation, Comput. Geom. 22 (1-3) (2002) 75–97.

[15] N. T. Folwell, S. A. Mitchell, Reliable whisker weaving via curve contraction, Eng. Comput. (Lond.) 15 (3) (1999) 292–302.

[16] K. Su, W. Chen, N. Lei, J. Zhang, K. Qian, X. Gu, Volume preserving mesh parameterization based on optimal mass transportation, Computer-Aided Design.

[17] H. M. Farkas, I. Kra, Riemann Surfaces, Springer, 2004.

[18] P. Knupp, Next-generation sweep tool: A method for generating all-hex meshes on two-and-one-half dimensional geomtries, in: 7th International Meshing Roundtable, 1998, pp. 505–513.

[19] M. L. Staten, S. A. Canann, S. J. Owen, Bmsweep: Locating interior nodes during sweeping, in: 7th International Meshing Roundtable, IMR 1998, 1998, pp. 7–18.

[20] S.-S. Liu, G. Rajit, Automatic hexahedral mesh generation by recursive convex and swept volume decomposition, in: 6th International Meshing Roundtable, 1997, pp. 347–364.

[21] A. Sheffer, M. Etzion, A. Rappoport, M. Bercovier, Hexahedral mesh generation using the embedded voronoi graph, Eng. Comput. (Lond.) 15 (3) (1999) 248–262.

[22] T. Blacker, The cooper tool, in: 5th International Meshing Roundtable, 1996.

[23] M. Hohmeyer, W. Christopher, Fully-automatic object-based generation of hexahedral meshes, in: 4th International Meshing Roundtable, 1995.

[24] D. White, L. Mingwu, S. Benzley, G. Sjaardema, Automated hexahedral mesh generation by virtual decomposition, in: 4th International Meshing Roundtable, 1995.

[25] K. Miyoshi, T. Blacker, Hexahedral mesh generation using multi-axis cooper algorithm, in: 9th International Meshing Roundtable, 2000.

[26] T. D. Blacker, R. J. Meyers, Seams and wedges in plastering: A 3-d hexahedral mesh generation algorithm, Engineering with Computers 9 (2) (1993) 83–93.

[27] M. Li, R. Tong, All-hexahedral mesh generation via inside-out advancing front based on harmonic fields, The Visual Computer 28 (6) (2012) 839–847.

[28] T. J. Tautges, T. Blacker, S. A. Mitchell, The whisker weaving algorithm: A connectivitybased method for constructing all-hexahedral finite element meshes (1995).

[29] F. Ledoux, J.-C. Weill, An extension of the reliable whisker weaving algorithm, in: 16th International Meshing Roundtable, 2007.

[30] J. Huang, Y. Tong, H. Wei, H. Bao, Boundary aligned smooth 3d cross-frame field, ACM Trans. Graph. 30 (6) (2011) 143.

[31] Y. Li, Y. Liu, W. Xu, W. Wang, B. Guo, All-hex meshing using singularity-restricted field, ACM Trans. Graph. 31 (6) (2012) 177.

[32] M. Nieser, U. Reitebuch, K. Polthier, Cubecover- parameterization of 3d volumes, Comput. Graph. Forum 30 (5) (2011) 1397–1406.

[33] L. Marechal, Advances in octree-based all-hexahedral mesh generation:handling sharp features, in: Proceedings of the 18th intl meshing roundtable, 2009, pp. 65–84.

[34] Y. Ito, A. Shih, B. Soni, Octree-based reasonable-quality hexahedral mesh generation using a new set of refinement templates, International for Numerical Methods in Engineering 77 (13) (2009) 189–1833.

[35] B. Lévy, Y. Liu, Lp centroidal voronoi tesselation and its applications, ACM Transactions on Graphics (SIGGRAPH conference proceedings)Patent pending - FR 10/02920 (filed 07/09/10).

[36] Y. He, H. Wang, C.-W. Fu, H. Qin, A divide-and-conquer approach for automatic polycube map construction, Computer & Graphics 33 (3) (2009) 369–380.

[37] J. Gregson, A. Sheffer, E. Zhang, All-hex mesh generation via volumetric polycube deformation, Computer Graphics Forum 30 (5).

[38] M. Nieser, U. Reitebuch, K. Polthier, CubeCover - Parameterization of 3D Volumes, Computer Graphics Forum 30 (5).

[39] J. Huang, Y. Tong, H. Wei, H. Bao, Boundary aligned smooth 3d cross-frame field, ACM Transaction on Graphics 30 (6) (2011) 143.

[40] Y. Li, Y. Liu, W. Xu, W. Wang, B. Guo, All-hex meshing using singularity-restricted field, ACM Transaction on Graphics 31 (6) (2012) 177.

[41] X. Gu, S.-T. Yau, Computational Conformal Geometry, International Press, 2008.

[42] K. Strebel, Quadratic Differentials, Springer-Verlag, 1984.

[43] J. Hubbard, H. Masur, Quadratic differentials and foliations, Acta Math. (142) (1979) 221–274.

[44] J. Liu, On the existence of jenkins-strebel differentials, Bull. London Math. Soc. 36 (2004) 365–377.

[45] X. Li, X. Gu, H. Qin, Surface mapping using consistent pants decomposition, IEEE Transaction on Visualization and Computer Graphics 15 (4) (2009) 558–571.